2006

Regulation of Mercury Resistance in the Crenarchaeote *Sulfolobus solfataricus*

James Schelert
University of Nebraska-Lincoln

Melissa Drozda
University of Nebraska-Lincoln

Vidula Dixit
University of Nebraska-Lincoln

Amanda Dillman
University of Nebraska-Lincoln

Paul H. Blum
University of Nebraska - Lincoln, pblum1@unl.edu

JOURNAL OF BACTERIOLOGY, Oct. 2006, p. 7141–7150
0021-9193/06/$08.00+0 doi:10.1128/JB.00558-06

Supporting information for this article is available following the references.

Vol. 188, No. 20

Regulation of Mercury Resistance in the Crenarchaeote *Sulfolobus solfataricus*†

James Schelert, Melissa Drozda, Vidula Dixit, Amanda Dillman, and Paul Blum*

George Beadle Center for Genetics, University of Nebraska—Lincoln, Lincoln, Nebraska

Received 19 April 2006/Accepted 6 August 2006

Mercuric ion, Hg(II), inactivates generalized transcription in the crenarchaeote *Sulfolobus solfataricus*. Metal challenge simultaneously derepresses transcription of mercuric reductase (*merA*) by interacting with the archaeal transcription factor aMerR. Northern blot and primer extension analyses identified two additional Hg(II)-inducible *S. solfataricus* genes, *merH* and *merI* (SSO2690), located on either side of *merA*. Transcription initiating upstream of *merH* at promoter *merHp* was metal inducible and extended through *merA* and *merI*, producing a *merHAI* transcript. Northern analysis of a *merRA* double mutant produced by linear DNA recombination demonstrated *merHp* promoter activity was dependent on aMerR to overcome Hg(II) transcriptional inhibition. Unexpectedly, in a *merA* disruption mutant, the *merH* transcript was transiently induced after an initial period of Hg(II)-mediated transcription inhibition, indicating continued Hg(II) detoxification. Metal challenge experiments using mutants created by markerless exchange verified the identity of the MerR binding site as an inverted repeat (IR) sequence overlapping the transcription factor B binding recognition element of *merHp*. The interaction of recombinant aMerR with *merHp* DNA, studied using electrophoretic mobility shift analysis, demonstrated that complex formation was template specific and dependent on the presence of the IR sequence but insensitive to Hg(II) addition and site-specific IR mutations that relieved in vivo *merHp* repression. Despite containing a motif resembling a distant ArsR homolog, these results indicate aMerR remains continuously DNA bound to protect and coordinate Hg(II)-responsive control over *merHAI* transcription. The new genetic methods developed in this work will promote experimental studies on *S. solfataricus* and other *Crenarchaeota*.

Heavy metals (class B; soft metals) are among the most toxic substances on earth. They are extremely poisonous at low concentrations and include mercury (Hg), cadmium (Cd), and lead (Pb). Among bacteria, active resistance to mercuric ion, Hg(II), is regulated by MerR, a unique representative of the winged helix-turn-helix (wHTH) family of bacterial transcription factors (4). MerR controls production of mercuric reductase (MerA) along with other related components (reviewed in reference 5). This protein acts as both a repressor and a metal-responsive activator of the mercury resistance genes by binding an operator sequence (*merO*) located between −10 and −35 hexameric promoter elements (3). In this conformation, MerR bends DNA towards itself in a manner like the catabolite activator protein and allows RNA polymerase to form an inactive but promoter-bound complex. In the activator conformation, Hg-MerR relaxes these bends, inducing DNA distortion at *merO* and an underwound spacer region (3). The magnitude and direction of this Hg-MerR-induced distortion comprises a positive control mechanism that reorients conserved promoter elements (2, 9).

Members of the phylum *Crenarchaeota*, including the thermoacidophile *Sulfolobus solfataricus*, inhabit metal-rich geothermal environments often containing high and naturally occurring levels of heavy metals. Proliferation under these conditions is accompanied by induction of active metal detoxification pathways (16) that include homologs of mercuric reductase, MerA, and the transcriptional regulator MerR (27). However, while regulated induction of gene expression in *Archaea* is not well understood, it relies on the use of numerous eukaryote-like general transcription components, including homologous promoter structures and orthologs of generalized transcription factors TBP and TFIIB, as well as an RNA polymerase II-like enzyme (reviewed in reference 20). TBP and TFB bind the archaeal promoter TATA box, forming a preinitiation complex, and acutely bend the DNA in a manner identical to that shown for eukaryotic promoters (17). Interestingly, archaeal genomes encode numerous bacteria-like regulatory factor sequences, suggesting an interplay occurs in these organisms between bacterial and archaeal transcription components. Since this interplay must accommodate the acutely bent DNA associated with the preinitiation complex, it is likely that archaeal gene-specific transcription factors employ unique mechanisms to regulate initiation frequency despite their sequence homology with bacterial proteins.

Genetic studies have demonstrated *S. solfataricus* MerA was required for Hg(II) reduction and for low-level metal resistance relative to that observed in bacteria (24). Since a *merR* disruption mutant exhibited elevated Hg(II) resistance and constitutive synthesis of the *merA* transcript, archaeal MerR (aMerR) appears to negatively regulate *merA* transcription. Though Hg(II) exposure induces expression of a resistance mechanism in *S. solfataricus*, it is also acutely toxic, because it inactivates transcription (10). In vivo Hg(II) challenge instantaneously blocked cell division and reduced overall RNA syn-

* Corresponding author. Mailing address: E234 Beadle Center, University of Nebraska, Lincoln, NE 68588-0666. Phone: (402) 472-2769. Fax: (402) 472-8722. E-mail: pblum1@unl.edu.

† Supplemental material for this article may be found as http://jb.asm.org/.

TABLE 1. Microbial strains and plasmids

Strain or plasmid	Genotype or sequence	Source or derivation
Strains		
PBL2000	Wild-type *S. solfataricus* strain 98/2	Lab collection
PBL2025	Δ(*SSO3004-3050*)	PBL2000 (24)
pBL2026	*merR*	PBL2025 (24)
PBL2038	*merR*::*lacS merA* Δ(nt 16–1362)	PBL2025 by linear recombination
PBL2036	*merI*::*lacS*	PBL2025 by markerless exchange
PBL2039	*merR*-IR1-SpeI	PBL2025 by markerless exchange
PBL2047	*merR*-IR2-XbaI	PBL2025 by markerless exchange
Plasmids		
pUC19	*bla*	New England BioLabs
pPB996	*merR*	pUC19 (this work)
pPB986	*merR*::*lacS*	pUC19 (24)
pPBMerA10	*merA*::*lacS*	pUC19 (24)
pPB1032	*merR*::*lacS merA* Δ(nt 16–1362)	pPB986 (this work)
pPB1015	*merI*	pUC19 (this work)
pPB1034	*merI*::*lacS*	pUC19 (this work)
pPB1035	*lacS*-KpnI	pUC19 (this work)
pPB1038	*lacS*-KpnI *merR*-IR1-SpeI	pPB1035 (this work)
pPB1051	*lacS*-KpnI *merR*-IR2-XbaI	pPB1035 (this work)

thesis while elevating rates of transcript degradation (10). In vivo or in vitro Hg(II)-treated whole-cell extracts failed to support in vitro transcription of *16S rRNAp* and *lacSp* promoters and could be rescued by addition of TFB to Hg(II)-treated cell extracts (10). Hg(II) treatment of TFB in vitro inactivated its ability to restore in vitro transcription activity of TFB-immunodepleted cell extracts (10). These findings indicated that Hg(II) toxicity in *S. solfataricus* was mainly the consequence of transcription inhibition due to TFB inactivation. Consequently, it is unclear how Hg(II) exposure could simultaneously stimulate *merA* transcription while blocking overall RNA synthesis. In the studies described here, several new genetic methods were developed and combined with standard RNA and DNA analytical approaches to investigate this question and to clarify the specific role of aMerR.

MATERIALS AND METHODS

Archaeal strains, cultivation, and mutant construction. Archaeal strains and plasmids used in this work are indicated in Table 1; primers are given in the supplemental material. *Sulfolobus solfataricus* strains were grown with aeration at 80°C in the medium of Allen (1) as modified by Brock et al. (8) at a pH of 3.0 in 250-ml screw-cap flasks as described previously (22, 30). Carbon and energy sources included 0.2% (wt/vol) sucrose (SM) or tryptone (RM) as indicated. Growth was monitored at a wavelength of 540 nm using a Cary 50 Bio, UV-visible spectrophotometer (Varian). When investigating the effect of mercuric ion, cells were typically grown to an optical density at 540 nm of 0.1, which corresponds to a previously established value of approximately 10^8 cells/ml. Cells were then treated with various concentrations of mercuric chloride (Sigma) from a freshly made 10 mM stock for the times indicated. Mutant strains were constructed using both new and previously established methods (24, 31). Electroporation was used to mobilize DNA into target cells, and strain PBL2025 (24) was used as the recipient.

Construction of the *merI* mutant. Construction of the *lacS*-disrupted *merI* mutant employed transformation by targeted recombination using plasmid pPB1015 as described elsewhere (24). The XhoI site located in *merI* of pPB1015 was created by overlap extension PCR (14) with primers merI-OL2-XhoI-F and merI-OL2-XhoI-R. The 5′ end of merI-OL2-XhoI-F begins 17 nucleotides (nt) downstream of the *merI* start codon and is complementary to merI-OL2-XhoI-R. Recombinant identity was confirmed by PCR of the modified *merI* allele, wild-type allele, and *lacS*-disrupted *merI* allele using primers merI-L-BamHI-F and merI-L-BamHI-R. The 5′ end of merI-L-BamHI-F is located 714 nt upstream of the *merI* start codon. The 3′ end of merI-L-BamHI-R is located 717 nt downstream of the *merI* stop codon. PCR and restriction analysis were used to verify the identity of the *merI* recombinant strain. Amplification of wild-type *merI* and flanking regions using primers merI-L-BamHI-F and merI-L-BamHI-R produced a single band of 1.80 kb (1,806 bp) that produced two fragments after XhoI digestion. Amplification of the disrupted *merI* locus in strain PBL2036 produced a single band of 3.60 kb (3,624 bp), approximately 1.80 kb larger than that observed with the undisrupted locus due to the presence of the inserted copy of *lacS*. This fragment produced three fragments after XhoI digestion of 0.75 kb (759 bp), 1.05 kb (1,053 bp), and 1.80 kb (1,806 bp) that represented the 5′ and 3′ ends of *merI* and the *lacS* insert, respectively.

Linear DNA transformation and construction of the *merRA* double mutant. Construction of the *merRA* double mutant employed transformation as described previously (24) using a linear DNA PCR amplicon. Primers used for PCR of the *merI* fragment were forward primer merI-L-BclI-F and reverse primer merI-L-KpnI-R. merI-L-BclI-F starts 1 nt downstream of the *merA* stop codon, and merI-L-KpnI-R starts 717 nt downstream of the *merI* stop codon. merI-L-BclI-F encodes an added BclI site, and merI-L-KpnI-R encodes an added KpnI site. Primers used for PCR of the *merRA* double mutant transformation fragment were forward primer merR-L-BamHI-F and reverse primer merI-L-BamH-R. merR-L-BamHI-F starts 546 nt upstream relative to the *merR* stop codon, and merI-L-BamHI-R starts 717 nt downstream relative to the *merI* stop codon. Both merI-L-BamHI-F and merI-L-BamHI-R encode an added BamHI site. Primers used for PCR verification of the *merRA* double mutant were forward primer merR-R-KpnI and reverse primers merI-R and merH2-R. merR-R-KpnI starts 19 nt upstream of the *merR* stop codon, and merI-R starts 49 nt downstream of the *merI* start codon. merH2-R starts 5 nt upstream of the *merA* start codon.

The pMerRS1 plasmid described previously (24) was digested with BclI (located 14 nt downstream from the 5′ end of *merA*) and KpnI (located 235 nt downstream from the BclI site and in the polylinker of pMerRS1) in order to remove a 235-bp *merA*-containing fragment. Plasmid pPB1032 was then constructed by insertion of a BclI-KpnI-digested PCR *merI* amplicon produced with primers merI-L-BclI-F and merI-L-KpnI-R and cloned into the BclI-KpnI sites of plasmid pMerRS1. The linear *merRA* double mutant PCR amplicon was produced with primers merR-L-BamHI-F and merI-L-BamH-R using the pPB1032 plasmid as the template DNA. This PCR amplicon was then transformed into strain PBL2025 as described previously. Amplification of the wild-type *merA* locus using primers merR-R-KpnI and merI-R produced a single fragment of 2.2 kb (2,216 bp). Amplification of the deleted *merA* locus in strain PBL2020 produced a single fragment of 2.6 kb (2,686 bp). Amplification of the wild-type *merR* locus using primers merR-R-KpnI and merH2-R produced a single fragment of 0.6 kb (665 bp). Amplification of the *lacS*-disrupted *merR* locus produced a fragment of 2.4 kb (2,473 bp).

Markerless exchange and construction of *merR* operator mutants. Markerless exchange employed a plasmid encoding a cloned copy of a modified DNA sequence together with a selectable but separable marker gene (*lacS*) to produce lactose-utilizing recombinant cells. Spontaneous lactose-nonutilizing segregants were recovered by recombination resulting from loss of the plasmid vector, selectable marker, and one of two copies of the target gene. Typically, four transformants were selected and monitored by screening for segregation of alleles. Unless otherwise noted, segregation frequency resulting in retention of the wild-type or modified allele was approximately 50%. Individuals retaining the modified allele of the target gene were identified using PCR of genomic DNA. In all cases only one mutant was chosen for further analysis.

Construction of the *merR*-IR mutants employed transformation by markerless exchange using plasmids pPB1038 and pPB1051. Primers used for PCR of the *lacS* fragment were forward primer LacS-KpnI-F and reverse primer LacS-KpnI-R. The 5′ end of LacS-KpnI-F starts 170 nt upstream of the *lacS* start codon, and the 3′ end of LacS-KpnI-R starts 165 nt downstream of the *lacS* stop codon. LacS-KpnI-F and LacS-KpnI-R each encode an added KpnI site.

Primers used for PCR of the *merR*-IR1 fragment were forward primer merR-L-BamHI-F and reverse primer merH-L-BamHI-R. The 5′ end of merH-L-BamHI-R begins 727 nt downstream of the *merA* start codon. Both merR-L-BamHI-F and merR-L-BamHI-R each encode an added BamHI site. The SpeI site located in the operator of the *merR*-IR1 fragment was created by overlap extension PCR (14) with primers merR-BS-SpeI-OL-F and merR-BS-SpeI-

OL-R. The 5′ end of merR-BS-SpeI-OL-F begins 25 nt upstream of the *merR* start codon and is complementary to merR-BS-SpeI-OL-R. Plasmid pB1035 was constructed by insertion of a KpnI-digested PCR *lacS* amplicon produced with primers LacS-KpnI-F and LacS-KpnI-R cloned into the KpnI site of pUC19. Plasmid pB1038 was constructed by insertion of a BamHI-digested PCR *merR*-IR2 amplicon into the BamHI site of pB1035.

The XbaI site located in the *mer* operator of the *merR*-IR2 fragment was created by overlap extension PCR (14) with primers merR-BS-XbaI-OL-F and merR-BS-XbaI-OL-R. The 5′ end of merR-BS-XbaI-OL-F begins 25 nt downstream of the *merR* start codon and is complementary to merR-BS-XbaI-OL-R. Plasmid pPB1051 was constructed by insertion of a BamHI-digested PCR *merR*-IR2 amplicon into the BamHI site of pPB1035.

PCR, restriction analysis, and DNA sequencing were used to verify the identity of the *merR*-IR recombinant strains. PCR of the modified *merR*-IR alleles and wild-type allele used primers merR-L-BamHI-F and merH-L-BamHI-R. Amplification of wild-type *merR* and flanking regions using primers merR-L-BamHI-F and merH-L-BamHI-R produced a single band of 1.9 kb (1,919 bp) that was not cut by XbaI. Amplification of the modified *merR*-IR1 sequence in strain PBL2039 produced a single band of 1.9 kb (1,923 bp). This fragment was cut by SpeI into two fragments of 0.94 kb (947 bp) and 0.98 kb (989 bp) that represented the 5′ and 3′ ends of the *merR*-IR1 insert, respectively. Amplification of the modified *merR*-IR2 sequence in strain PBL2047 produced a single band of 1.9 kb (1,923 bp). This fragment was cut by XbaI into two fragments of 0.94 kb (947 bp) and 0.98 kb (989 bp) that represented the 5′ and 3′ ends of the *merR*-IR2 insert, respectively. DNA sequencing of the *merR*-IR1 and *merR*-IR2 PCR amplicons also confirmed the identity of the respective mutations.

DNA cloning, PCR, and plasmid transformation of *Escherichia coli* were performed as described elsewhere (13, 21). DNA sequencing was as described previously (23). DNA and RNA concentrations were measured using either a DyNA Quant 200 fluorometer (Hoefer) or a UV-visible spectrophotometer Genesys 2 (Spectronics). All manipulations of RNA were as described previously (6, 12). Protein concentrations were measured using the BCA protein assay reagent kit (Pierce). Unless otherwise indicated, all chemicals were obtained from common chemical suppliers.

Northern blot analysis. RNA extraction and Northern hybridization using antisense riboprobes were performed as described elsewhere (6, 12). RNAs were detected by autoradiography on X-Omat AR film (Kodak). Digital images were acquired using a gel documentation system GDS7600 (UVP). Scanning densitometry of the images was performed using GelBase-Pro software (UVP). The *7S RNA* probe was prepared as described elsewhere (6). The *merA* probe was prepared by PCR amplification using chromosomal DNA and primers MerA-F and MerA-R that were complementary to positions 133 to 161 and 773 to 801, respectively, in the *merA* coding region. The 640-bp fragment was cloned at the XbaI and SphI sites of pT7T3/18U (Pharmacia). In riboprobe synthesis, *merA* was linearized using SmaI, and T3 RNA polymerase was used for transcription to produce a ^{32}P-labeled antisense RNA. The *merH* probe was prepared by PCR amplification using primers MerH-2F and MerH-2R. The 5′ end of MerH-2F is located 3 nt upstream of the *merH* start codon, and the 3′ end of MerH-2R is located 18 nt upstream of the *merH* stop codon. The 184-bp fragment was cloned at the EcoRI and HindIII sites of pT7T3/18U (Pharmacia). In riboprobe synthesis, *merH* was linearized using EcoRI, and T3 RNA polymerase was used to transcribe a ^{32}P-labeled antisense RNA. The *merI* probe was amplified by PCR using primers MerI-2F and MerI-3R, which were complementary to positions 1 to 34 and 341 to 368 relative to the *merI* coding region. The 368-bp fragment was cloned into EcoRI and PstI sites of pT7T3 and linearized with EcoRI. A labeled antisense RNA was transcribed using T3 RNA polymerase.

Primer extension analysis. The *merH* transcript was subjected to primer extension using primer MerH-PE, which is complementary to positions 64 to 84 downstream of the *merH* start codon. The primer extension oligonucleotide was labeled at the 5′ end with [γ-^{32}P]ATP using T4 kinase (USB) as described elsewhere (6, 29). The labeling reaction was terminated by EDTA addition followed by heating at 65°C. The labeled primer was purified using a Sep-Pak C_{18} cartridge (Waters), dried, and resuspended in 10 μl of 10 mM pH 8.0 Tris-Cl, 1 mM EDTA. A typical reaction yielded 10 μl of 10^6-cpm/μl-labeled oligo, and 1 μl of this oligo was used for each reverse transcription reaction. Reverse transcription was performed as described previously (6, 29) with modifications. Samples of total RNA (20 μg) were hybridized with the labeled primer in 150 mM $MgCl_2$, 10 mM Tris-Cl pH 8.3, and 1 mM EDTA, heated at 65°C for 90 min, and cooled to allow primer annealing. The mixture was adjusted to 20 mM Tris-Cl pH 8.3, 10 mM $MgCl_2$, 0.5 mM dithiothreitol, 0.15 mg/ml actinomycin D, 0.15 mM deoxynucleoside triphosphates, and 5 U of avian myeloblastosis virus reverse transcriptase (Pharmacia) was added. The reaction mixture was incubated for 1 h at 42°C and terminated by addition of 17.5 ng/ml salmon sperm DNA and 14 ng/ml RNase A followed by incubation for 15 min at 37°C. The reaction was extracted with phenol-chloroform (1:1), and primer-extended DNA was recovered by ethanol precipitation, dried, and resuspended in the Stop solution of the T7 Sequenase version 2.0 DNA sequencing kit (Amersham). The primer extension primer also was used to generate the sequencing ladder for mapping the start site of transcription of *merHp* and *merIp.* The template used to generate the DNA sequencing ladder for *merAp* primer extension mapping was plasmid pPBMerA10. DNA sequencing reaction products were separated on pre-equilibrated 8% (wt/vol) denaturing polyacrylamide sequencing gels as described previously (23).

EMSA of *merHp*. A 328-bp region spanning the *merHp* sequence was amplified from wild-type *S. solfataricus* or PBL2039, the mutant strain containing the *merR*-IR1 sequence, using primers MerA2-F and MerH-R. MerA2-F starts 325 nt upstream of the *merA* start codon and has an added EcoRI site, and MerH-R starts 4 nt upstream of the *merA* start codon. Template (100 ng) was end labeled using [γ-^{32}P]ATP and T4 polynucleotide kinase (USB) at 37°C for 60 min and terminated by the addition of 0.5 M EDTA pH 8.0, followed by incubation at 65°C for 5 min. The labeled oligonucleotide was recovered using phenol-chloroform (1:1) extractions followed by ammonium acetate and ethanol precipitation. Radiolabeled DNA was resuspended in 20 μl deionized distilled water, and its radioactivity was calculated using a Beckman LS1701 scintillation counter. Electrophoretic mobility shift assay (EMSA) reaction components were combined in a 10× buffer containing 0.5 M Tris-Cl pH 8.0, 250 mM $MgCl_2$, 10 mM EDTA, prepared using diethyl pyrocarbonate-treated deionized distilled water, along with varying amounts of recombinant MerR protein, 1.0 μg poly(dI-dC) (Sigma), 1 mM dithiothreitol (Invitrogen), and deionized distilled water to a final volume of 15 μl. Reaction mixtures were incubated at 50°C for 10 min. Probe was added to the mixtures at 10^6 cpm/μl and incubated for 20 min at 50°C. After incubation, glycerol was added to the reaction mixtures at 10% (vol/vol), and samples were loaded on a 6% (29:1 acrylamide-bisacrylamide), 1% glycerol, 1× Tris-borate-EDTA (TBE) gel using a Dual gel electrophoresis system (Owl). Electrophoresis was at 100 V for 3 h, and the gels were dried for 30 min at 80°C and used to expose X-ray film. Competition assays were performed using an unlabeled 328-bp fragment encoding the *merHp* sequence in molar excess as specific competitor. Nonspecific competitor DNA used was an unlabeled 176-bp *merA* fragment amplified using forward primer merAsense2 and reverse primer merAantisense. The 5′ end of merAsense2 begins 336 nt downstream of the *merA* start codon, and the 3′ end of primer merAantisense begins 511 nt downstream of the *merA* start codon. A mutant template with the 36 nt spanning the *mer* operator sequence deleted, called *merHp*-IRdel36, was created using primers merIR-OL-F2 and merIR-OL-R paired with merR-L-BamHI-F and merH-L-BamHI-R, respectively. The 5′ end of merIR-OL-F2 is located 30 nt downstream of the *merR* start codon. The 5′ end of merIR-OL-R is located 40 nt upstream of the *merH* start codon. For EMSA using Hg(II), MerR protein (139 nM) was first incubated for 10 min at 50°C, followed by addition of probe (33 pM) and further incubation for 10 min. Hg(II) was added after the binding reactions in amounts resulting in 0.1, 1.0, and 10.0 μM, and incubation was continued for 10 min at 50°C.

Preparation of recombinant aMerR. The *S. solfataricus merR* open reading frame (SSO2688) was amplified from genomic DNA using *Taq* polymerase (Invitrogen) and oligonucleotide primers MerR-F and MerR-R (24). The PCR amplicon was digested with NcoI and XhoI and ligated into pET28b (Novagen), creating plasmid pPB996. *E. coli* strain BL21 Rosetta (Novagen) was transformed with pPB996 for expression of recombinant C-terminal hexahistidine-tagged MerR. For preparation of recombinant MerR, cells were grown to an optical density at 600 nm of 0.1 and expression was induced by addition of 0.5 mM isopropyl-β-D-thiogalactopyranoside followed by a 3-h additional incubation. Cells were harvested by centrifugation, resuspended in 50 mM Tris-HCl pH 7.8, 0.5 M NaCl, 10% glycerol, 10 μM β-mercaptoethanol (buffer A), and lysed by sonication followed by centrifugation. The soluble extract was heated at 80°C for 20 min and centrifuged at 10,000 × *g* for 20 min to remove denatured proteins. All glassware and reagents used for MerR purification were made RNase free by baking at 180°C for 4 h or by treatment with DEPC. The supernatant was applied to a 1.0-ml Ni^{2+}-nitrilotriacetic acid agarose bead column (QIAGEN). The column was equilibrated with 10 column volumes of buffer A, and supernatant was then loaded followed by a wash with 5 column volumes of buffer A plus 75 mM imidazole. MerR eluted in 5 column volumes of buffer A plus 75 mM imidazole as indicated by analysis of fractions on sodium dodecyl sulfate-polyacrylamide gel electrophoresis after staining with Coomassie blue R250. Protein was concentrated using Centricon YM-3 or YM-10 (Amicon) filters prior to storage of aliquots at −80°C.

Alignment of the MerR operator. Sequences were identified with NCBI advanced BLASTn (expect value of 1,000; size 7) using the full genome sequences

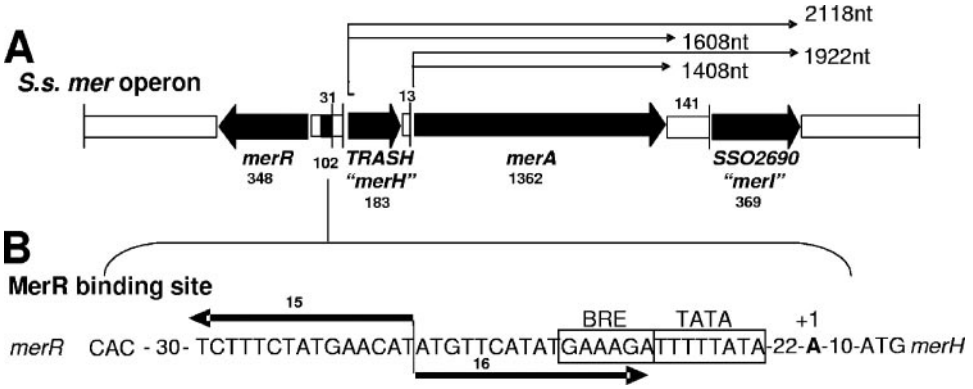

FIG. 1. Components of the *S. solfataricus mer* operon and *mer* operator. A. Components of the *S. solfataricus mer* operon. Nucleotide lengths are indicated for the open reading frames (filled arrows) and intergenic regions (open boxes). Promoters and estimated unprocessed transcript lengths are indicated (thin arrows). B. Sequence of the *mer* operator (divergent thin arrows), BRE and TATA elements (boxes), *merH* transcription start site (bold), and *merR* and *merH* initiator codons.

of *Sulfolobus acidocaldarius*, *Sulfolubus tokodai*, and *S. solfataricus*. ClustalW was used to create the multiple-sequence alignment.

RESULTS

Composition and transcription of the archaeal *mer* operon. In previous studies (24), primer extension mapping identified the 5′ end of the *merA* transcript 7 nt upstream of the *merA* start codon in a region lacking a canonical archaeal promoter (Fig. 1). Despite this finding, in vitro transcription analysis using a DNA template encoding this region failed to produce a specific start site, while a *16S rRNA* promoter template could (V. Dixit and P. Blum, unpublished). This raised the possibility that an alternate promoter was used in vivo at a site located further upstream. Consistent with this possibility was the identification of a small open reading frame annotated as a putative metal binding peptide encoding a "TRASH" domain in the *S. solfataricus mer* region (Fig. 1) (11). The TRASH domain is encoded within a 180-nt sequence, SSO10899, positioned 16 nt 5′ to the *merA* start codon and out of frame with regards to *merA* (25). Sequence comparisons indicated it lacked homology with bacterial *merT* or the *merP*-like N-terminal domains found on some bacterial MerA proteins. Presence of a conserved metal binding motif suggested instead that it could be involved in Hg(II) mobilization by acting as a metal chaperone. To test whether SSO10899 was expressed in response to Hg(II) challenge, Northern blot analysis was conducted. Hybridization of total RNA from Hg(II) challenged wild-type cells, using a riboprobe complementary to SSO10899, detected two transcripts of the identical sizes as those seen previously using a *merA* riboprobe (24) (Fig. 2A). These transcripts differed in size by approximately 400 nt. The similarity in transcript sizes detected using riboprobes complementary either to *merA* or SSO10899 indicated SSO10899 was cotranscribed with *merA* from a start site further upstream. The SSO10899 open reading frame was thus renamed *merH*.

On the 3′ side of *merA* is another open reading frame, SSO2690 (25). This gene encodes a small protein of 122 residues and is separated from *merA* by a 142-nt intergenic region. SSO2690 has several characteristics of interest, including an acid-rich domain in its N-terminal region reminiscent of the acid blob domains found in eukaryotic activators and a zinc finger domain in its C-terminal region with the motif Cx_2Cx_9 CxC. This protein is a conserved crenarchaeotal protein with homologs of nearly identical size in the related organism *Sulfolobus tokodai* (70% identity in the C terminus) and *Acidianus ambivalens* (80% identity in the C terminus). Hybridization of

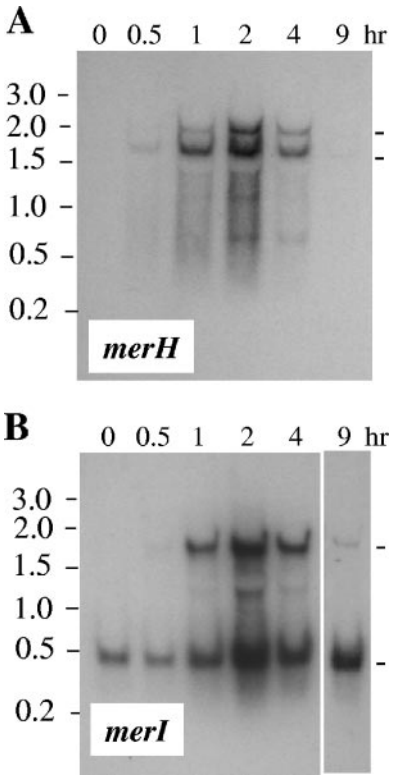

FIG. 2. Northern blot analysis of *merH* and *merI* expression during mercury challenge. A. Northern blot analysis of *merH*. B. Northern blot analysis of *merI*. Samples were removed at the times indicated from a culture treated with 0.3 μM mercuric chloride and analyzed for mRNA content using *merH* and *merI* riboprobes, respectively. Major transcripts are indicated (dashes). Culture doubling time ranged from 8 to 10 h.

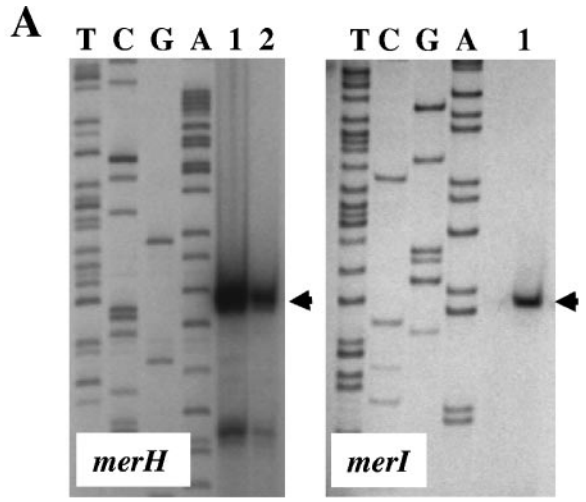

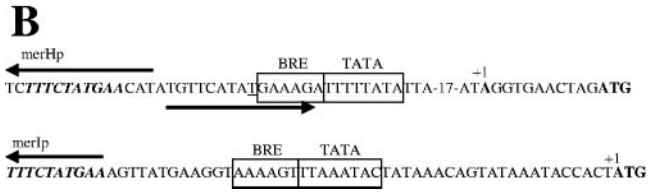

FIG. 3. Primer extension and DNA sequence analysis of *merH* and *merI* promoter regions. A. Primer extension analysis. RNA was obtained from cultures 4 h after treatment with 0.3 μM mercuric chloride. B. Promoter sequences. The location of the operator at *merHp* and matching half-repeat at *merIp* are indicated (arrows). The TBP binding site (TATA box octamer) and TFB binding site (BRE hexamer) are indicated by the boxed regions. Transcription start sites (+1) and start codons (bold) are indicated.

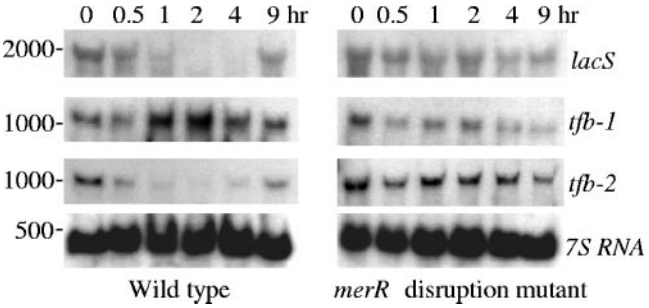

FIG. 4. Effect of mercuric reductase overproduction on Hg(II)-challenged mRNA abundance. Samples were removed at the times indicated from the wild-type and the *merR* disruption mutant strains treated with 0.3 μM mercuric chloride and then analyzed for mRNA content. Northern blots were analyzed using four different probes (*lacS*, *tfb-1*, *tfb-2*, and *7S RNA*); *7S RNA* was used as an internal control. Transcript sizes are indicated on the left.

total RNA from Hg(II)-challenged wild-type cells using an SSO2690 riboprobe detected a transcript that was the same size as the smaller of two large transcripts seen previously using both the *merH* riboprobe and the *merA* riboprobe (24) (Fig. 2B). A second transcript sufficient in size to encode SSO2690 was also observed. This smaller transcript was constitutively expressed at a low level, but following Hg(II) exposure its abundance increased. These results indicate SSO2690 is cotranscribed in a mercury-responsive manner with *merH* and *merA* from a promoter located upstream of *merH* and, separately, from its own promoter. SSO2690 was therefore renamed *merI*. These data revise the composition of the *S. solfataricus mer* locus to include four genes (Fig. 1).

Primer extension analysis was used to determine the transcription start sites located upstream of *merH* and upstream of *merI* (Fig. 3A). The 5′ end of the transcript initiating upstream of *merH* was 11 nt from the *merH* start codon. The 5′ end of the transcript initiating upstream of *merI* occurred at the first position of the *merI* start codon, indicating this transcript was a leaderless mRNA. In previous studies, in vivo primer extension analysis mapped the 5′ end of the *merA* transcript immediately upstream of *merA* and 3′ to the *merH* coding region (24). The *merH* Northern and primer extension data, however, indicated that a transcript encoding *merA* could initiate upstream of *merH* at a promoter called *merHp*. Taken together these data suggested that a primary transcript initiated at *merHp* was endonucleolytically processed to produce the 5′ end near *merA* and that *merHp* rather than *merAp* is the main *mer* promoter.

The *mer* operator sequence. Sequence examination of the region upstream of *merHp* identified a 31-nt inverted repeat (Fig. 3B, top) as the putative binding site for aMerR. The right half of this repeat overlaps the putative TFB binding site (BRE) of *merHp* and contains one additional T immediately adjacent to the BRE. The internal 18 nt of this sequence includes a perfect inverted repeat with 8-nt half-sites and a 2-nt central spacer. In bacteria, a shorter inverted repeat comprises the binding site for MerR and is located between divergently transcribed −10 and −35 boxes (5). The location of the *S. solfataricus* sequence in an upstream location suggests a mechanism for how aMerR may control and possibly protect generalized transcription factors bound at *merHp* from transcription inhibition during Hg(II) exposure. A large segment of this inverted repeat sequence (10 contiguous positions out of 15) is also found upstream of the putative *merI* promoter (Fig. 3B, bottom), suggesting aMerR may bind both locations and mediate transcription in response to Hg(II) exposure.

Effect of MerA on mRNA abundance. Efforts to gain an understanding of the mechanism underlying Hg(II) as an inducer of *mer* expression were complicated by the simultaneous effect of this metal as a general inhibitor of transcription (10). Accumulation of mercuric reductase (MerA) could impact this process by accelerating metal detoxification (24). To test this hypothesis, a strain that constitutively expressed *merA* (MerR deficient) was used to measure transcription inhibition (10) relative to an otherwise isogenic wild-type strain by evaluating mRNA abundance for selected genes. Transcript abundance levels of several genes, including *lacS*, *tfb-1*, *tfb-2*, and *merA*, were evaluated in cells overproducing MerA (Fig. 4). Elevation of MerA levels was achieved using a strain with an inactivated copy of *merR*. Batch cultures grown in SM were treated with 0.3 μM mercuric chloride, and samples were removed for analysis at times thereafter. The signal recognition particle, 7S RNA, was used to standardize mRNA band intensity as described previously (6). In the *merR* disruption mutant, transcript levels for all genes remained virtually unaffected by Hg(II) challenge throughout the time course. In the wild-type strain, all transcripts were detected at 0 and 0.5 h; however, *lacS* and *tfb-2* transcript levels dropped

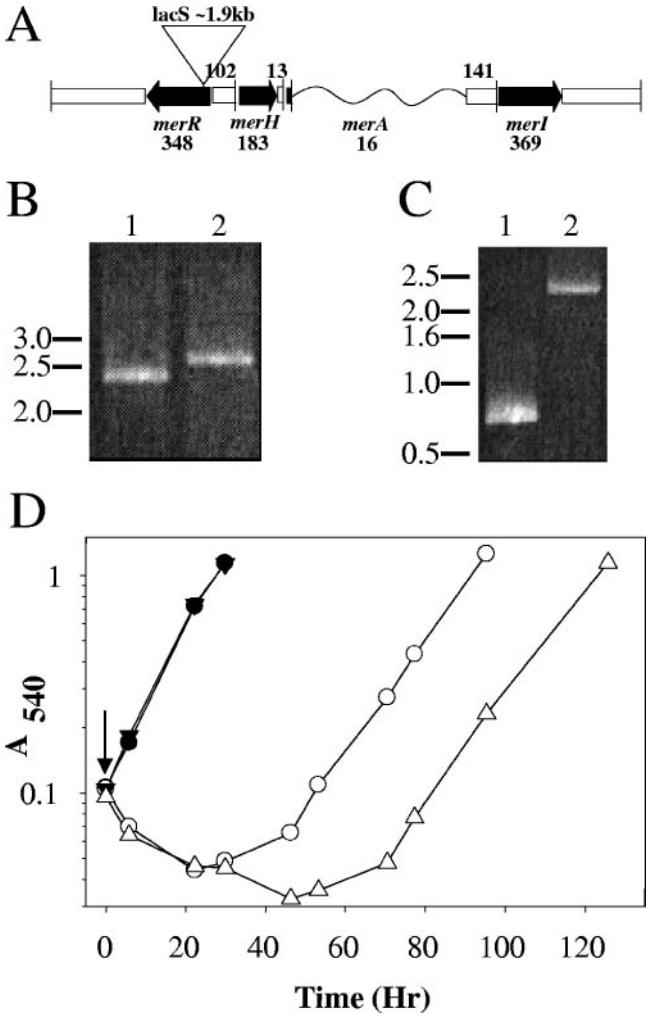

FIG. 5. Linear DNA recombination and the *merRA* double mutant. A. Schematic representation of the linear DNA used to create the *merRA* double mutant encoding the disrupting copy of *lacS* (triangle) in *merR* and deletion of *merA* (wavy line). The ORFs with corresponding lengths in nucleotides and directions of transcription are indicated (block arrows). Each end of the fragment encodes an added BamHI restriction site. B. PCR analysis of the entire *mer* operon and flanking sequences in the wild type and *merRA* double mutant. Lane 1, wild type; lane 2, *merRA* double mutant. Sizes (in kb) are indicated on the left. C. PCR analysis of the entire *merR* locus and flanking sequences in the wild type and *merRA* double mutant. Lane 1, wild type; lane 2, *merRA* double mutant. Sizes (in kb) are indicated on the left. D. Response of the *merRA* double mutant to Hg(II) challenge. Cells were grown in SM to a density of 10^8 cells/ml and challenged with 0.5 μM mercuric chloride at the time indicated (arrow). Symbols: triangles, *merRA* double mutant; circles, wild type; filled symbols, untreated cultures; open symbols, treated cultures.

sharply at 1, 2, and 4 h. After 9 h of Hg(II) exposure, each of these mRNAs was again detected. Interestingly, the level of *tfb-1* mRNA was increased at 1 and 2 h in the wild-type strain during Hg(II) challenge. These results indicate high intracellular levels of MerA suppress the Hg(II)-mediated reduction in transcript abundance arising from inhibition of generalized transcription (10, 24), and they support the use of strains lacking this gene in subsequent studies.

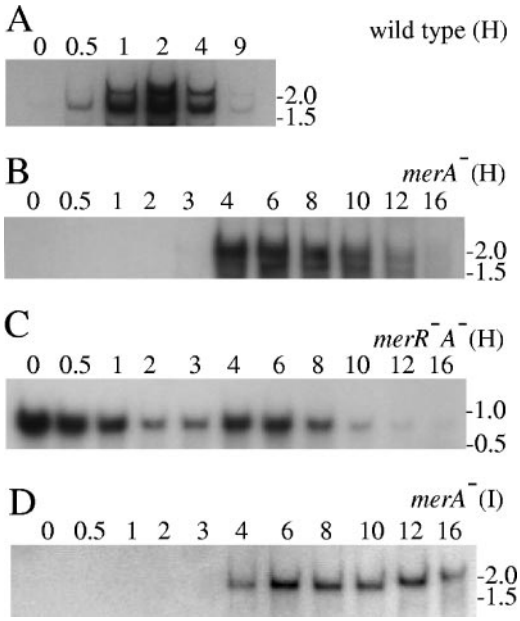

FIG. 6. Relative abundance of Hg(II)-challenged *merH* mRNA in multiple genetic backgrounds. Samples treated with 0.3 μM mercuric chloride were removed from the cultures listed at the times indicated and analyzed for mRNA content. Northern blots were probed either with *merH* (A, B, and C) or *merI* (D) riboprobes. The genetic backgrounds of strains used for RNA extraction are indicated above each panel.

MerR and Hg(II)-resistant transcription. The *mer* genes undergo induction when transcription of other genes is inhibited (10, 24). This suggests *mer* responds in a fundamentally different way to metal challenge and implicates a role for MerR in this process. The contribution of MerR in Hg(II)-resistant transcription of *merHp* was investigated using a double mutant encoding a *merA* deletion in a *merR*::*lacS* disruption mutant background (strain PBL2026) (24).

The *merRA* double mutant was created using linear DNA recombination to replace wild-type *merA* located in the chromosome with a deleted version (Fig. 5A). A PCR product was transformed into the *merR* disruption mutant that encompassed the *lacS*-disrupted *merR* gene, *merH*, a deletion of *merA* spanning nt 16 to 1362, SSO2690, and its flanking regions. Recombinants were recovered by selection for lactose utilization and characterized using PCR and DNA sequencing. The identity of the *merRA* double mutant was confirmed by PCR analysis and DNA sequencing (Fig. 5B and C). To assess the physiological consequence of *merA* deletion in the absence of *merR*, the response of the *merRA* double mutant to Hg(II) challenge was compared to that of the otherwise-isogenic wild-type strain (Fig. 5D). Both strains were grown in SM and at a cell density of 10^8 cells/ml, and 0.5 μM Hg(II) was added to each culture. Untreated cultures of both strains were included as controls. Growth of the wild-type strain exhibited a lag followed by a slightly reduced rate of growth, while the *merRA* double mutant exhibited a significantly longer lag followed by a slightly reduced rate of growth. Recovery of the mutant suggests Hg(II) was redistributed and possibly reduced by other cellular reductases or was lost to cellular thiols.

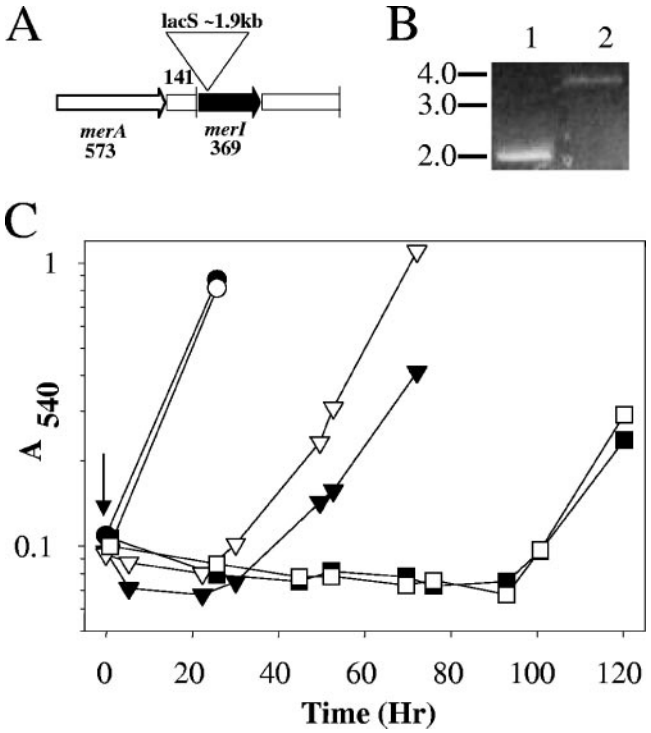

FIG. 7. Targeted recombination and the *merI* mutant. A. Schematic representation of the DNA used to create the *merI* mutant encoding the disrupting copy of *lacS* (triangle) in *merI*. The ORFs with corresponding lengths in nucleotides and directions of transcription are indicated (block arrows). B. PCR analysis of the *merI* locus and flanking regions in the wild type and *merI* mutant. Lane 1, wild type; lane 2, *merI* disruption mutant. Sizes (in kb) are indicated on the left. C. Adaptive response of the *merI* mutant to Hg(II) challenge. Cells were grown in SM to a density of 10^8 cells/ml and challenged with mercuric chloride as indicated in Materials and Methods, at the time indicated (arrow). Symbols: open symbols, *merI* mutant; filled symbols, wild type; circles, untreated cultures; triangles, adapted cultures; squares, unadapted cultures.

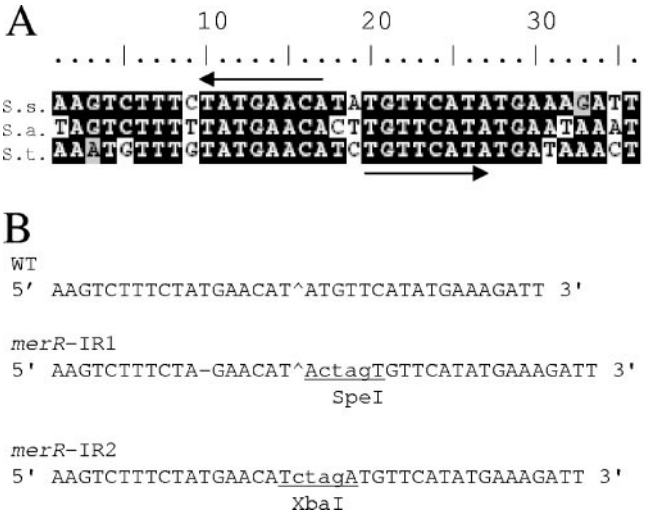

FIG. 8. The MerR operator. A. Alignment of the MerR operator with *Sulfolobus acidocaldarius* (S.a.) and *Sulfolobus tokodai* (S.t.). The conserved operator sequence spans 18 nt and includes 8-nt palindromic arms (arrows) flanking a central 2-nt T-containing spacer. The percent identity between each of the conserved operator sequences is 16/18 (88% identity). When full-length alignments are considered, the identity values are greater than 80% (*S. solfataricus*/*S. acidocaldarius*, 29/36 [80.56%]; *S. solfataricus*/*S. tokodai*, 29/36 [80.55%]). B. Mutagenesis of the *mer* operator. A schematic representation of the location and sequence of the modified operator sequences is shown. Mutant nucleotides are indicated in lowercase. WT, wild type. Encoded restriction sites (underlined) are indicated below the sequence, as are the points of symmetry (circumflex) and nucleotide deletion (dash).

Northern blot analysis was conducted to test the dependence of *merHA* transcription on the presence of MerA and MerR (Fig. 6). Batch cultures grown in SM were again treated using 0.3 μM Hg(II), and samples were removed for analysis at times thereafter using either *merH* or *merI* riboprobes. In the wild-type strain (Fig. 6A), the *merH* transcript was undetected at 0 h, very slightly after 0.5 h, then more strongly after 1, 2, and 4 h, and became undetectable after 9 h in a pattern similar to that reported previously (24). In the *merA* disruption mutant (Fig. 6B), *merH* transcript levels exhibited metal induction but in a delayed manner, becoming detectable after 4 h and undetectable after 16 h. A similar pattern of RNA abundance was evident when samples were probed using a *merI* riboprobe, as expected for this multicistronic RNA (Fig. 6D). In the *merRA* double mutant, *merH* transcript abundance was initially high (constitutive expression) but decreased significantly over the next 3 h (Fig. 6C). Thereafter, *merH* transcript levels increased in a transient manner, as observed for the *merA* disruption mutant, but then became undetectable after 12 to 16 h rather than resuming the constitutive and high pattern of abundance observed in the other genetic backgrounds. In all cases, after extended periods of incubation, the metal-treated strains resumed growth. These data demonstrate that in the absence of MerR, synthesis of the *merH* transcript in Hg(II)-treated cells is inhibited, as observed for other transcripts, like *lacS* (Fig. 4). At the same time, transient but delayed induction of the *merH* transcript in both the *merA* and *merRA* double mutants revealed the presence of a secondary pathway for Hg(II) detoxification which may result from other cellular reductases or cellular thiols.

Role of SSO2690 (*merI*). The role of *merI* in the Hg(II) resistance phenotype was investigated by creating and characterizing a mutant strain encoding a *merI*::*lacS* disruption (Fig. 7A). Disruption of *merI* used a strategy similar to that employed for the *merR* disruption in strain PBL2025 (24). Identity of the *merI* mutant was confirmed by PCR analysis and DNA sequencing (Fig. 7B). To assess the physiological consequence of gene disruption, the response of the mutant strain to Hg(II) challenge was compared to that of the otherwise-isogenic wild-type strain, both growing in SM, using unadapted and 0.5 μM Hg(II)-preadapted cells as described previously (24). All cultures at cell densities of 10^8 cells/ml were challenged with 0.5 μM (unadapted) or 1.5 μM (adapted) mercuric chloride (Fig. 7C). Untreated cultures of both strains were included as controls. No significant difference in patterns of growth was apparent between the two strains under either treatment regimen.

Construction and analysis of the *merR* operator mutants. Multiple sequence alignments of the operator, derived from the sequenced genomes of three *Sulfolobus* species, were examined (Fig. 8A). Except for the central two nucleotides, the

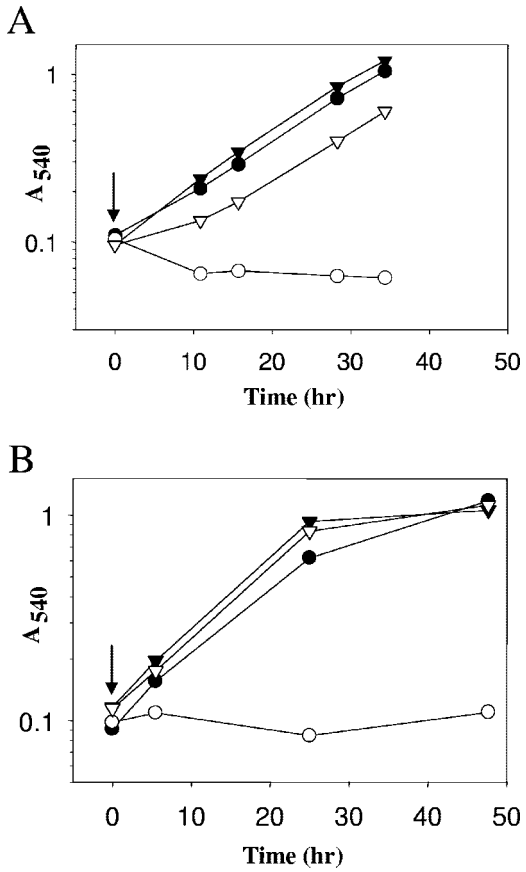

FIG. 9. Response of the *mer* operator mutants to Hg(II) challenge. Cells were grown in SM and challenged with 0.5 μM mercuric chloride (arrow). A. Cultures were *merR*-IR1 mutant (inverted triangles) and wild type (circles). B. Cultures were *merR*-IR2 mutant (inverted triangles) and wild type (circles). Filled symbols, untreated cultures; open symbols, treated cultures.

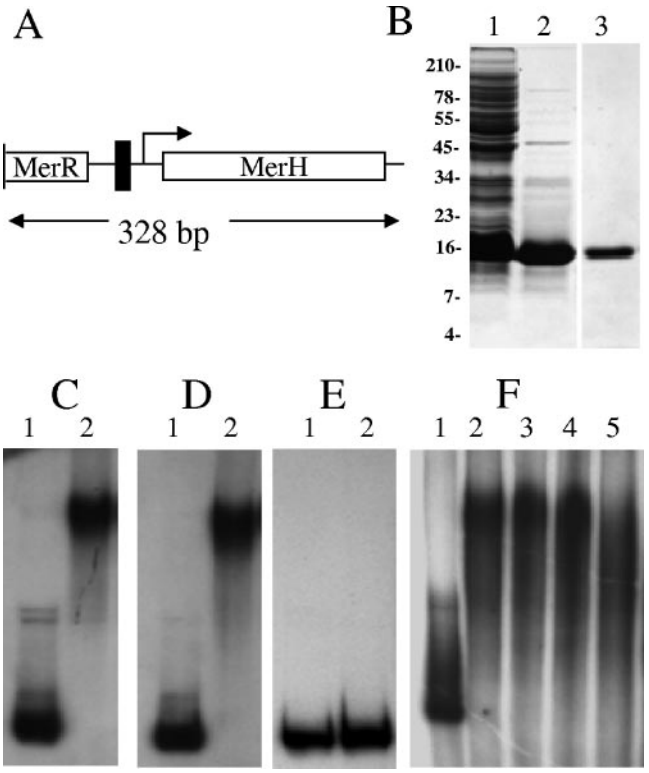

FIG. 10. EMSA of *merHp* using purified MerR. A. Schematic of the *merHp* EMSA probe. The location of *merR*-IR is indicated (filled box). B. Purification of recombinant aMerR. Lane 1, total cell extract; lane 2, heat-fractionated clarified supernatant; lane 3, affinity-purified protein. C. Mobility of the wild-type *merHp* probe. Lane 1, probe only; lane 2, probe with MerR. D. Mobility of the *merHp*-IR1 probe. Lane 1, probe only; lane 2, probe with MerR. E. Mobility of the *merHp*-IRdel36 probe. Lane 1, probe only; lane 2, probe with MerR. F. Effects of increasing concentrations of mercuric chloride on the mobility of the wild-type *merHp* probe with MerR. Lane 1, probe only; lanes 2 to 5, probe, MerR, and 0, 0.1, 1.0, and 10.0 μM mercuric chloride, respectively (added after the binding reactions). In all EMSA reactions, MerR was present at 139 nM while the *merHp* EMSA probe was present at 33 pM.

core 18-nt *mer* operator is conserved in all three *Sulfolobus* species. This suggests the flanking 8 nt in each half of the operator are critical for MerR binding. It is possible the central 2 nucleotides are necessary as a spacer for binding and function of an aMerR homodimer. Mutant strains encoding mutations of this sequence were then created and characterized.

Site-specific mutagenesis coupled with markerless exchange was used for the first time with this organism to introduce mutations in both halves of the operator (*merR*-IR1) or that separated the two halves by 4 nt (*merR*-IR2), thereby rotating the respective segments to opposite sides of the DNA helix (Fig. 8B). The *lacS*-deficient strain, PBL2025, allows for efficient recombination of unmarked mutations onto the chromosome via markerless exchange (7, 19) using *lacS* as a selectable marker. To perform markerless exchange, the desired mutation was first cloned into a suicide plasmid having *lacS* inserted in the vector backbone. The resulting plasmid was then used to transform PBL2025 to lactose utilization. Transformants arose by integration into the host chromosome via homologous recombination between the plasmid-borne mutant allele and the chromosomal wild-type allele. Integration cannot occur at the *lacS* locus, because PBL2025 carries a deletion of this region (24). The resulting merodiploids were unstable due to the extra copy of the mutant allele. Recombinants which have resolved the merodiploid state (and therefore have lost the integrated vector) result in either wild-type or mutant individuals, depending on where the resolving recombination event occurs. These alleles can readily be distinguished by screening for the lactose utilization phenotype. Next, genotypic analysis was used to confirm the identity of the mutants. Both operator mutants and the *merR* disruption mutant used as a control exhibited constitutive resistance to a challenge of 0.5 μM mercuric chloride, while the same dose blocked growth of the wild-type strain (Fig. 9). Since overexpression of mercuric reductase reduces sensitivity to Hg(II), constitutive Hg(II) resistance indicates the *merR*-IR mutants have this property and are analogous to the *merR* disruption mutant that has been described previously (24).

Electrophoretic mobility shift analysis of aMerR and *merHp*. Physiological analysis of the mutants harboring altered operator sequences indicated this sequence was the binding site for aMerR. To study further the interaction between

aMerR and this region, EMSA was conducted using a radiolabeled 328-bp DNA probe spanning the *merHp* region (Fig. 10A) and purified recombinant aMerR (Fig. 10B). Small amounts of aMerR (139 nM) were sufficient to shift this probe (33 pM) (Fig. 10C). Competition experiments demonstrated that the interaction between aMerR and the *merHp* probe was specific, as the complex was competed by a 300-fold excess of specific competitor and not by a 1,000-fold excess of nonspecific competitor (data not shown). Since the in vivo phenotype of the *merR*-IR1 mutant suggested aMerR could no longer repress transcription, the interaction of aMerR with this mutant sequence in vitro was examined. EMSA was performed using a radiolabeled DNA probe encoding the *merR*-IR1 allele of the same length and molarity as the wild-type sequence. Interestingly, nominal amounts of aMerR (139 nM) again formed a complex (Fig. 10D). In light of this result, aMerR binding to a second mutant DNA probe having the entire operator sequence deleted by removal of 36 nt (*merHp*-IRdel36) was tested under identical conditions. In this case, no complex was formed, indicating the protein-DNA interaction was dependent on the presence of the operator sequence (Fig. 10E). Finally, to address the potential impact of Hg(II) on complex formation, various concentrations of Hg(II) were used to treat preformed aMerR/*merHp* DNA complexes. Complex formation remained evident and therefore was insensitive to metal exposure despite molar ratios of Hg(II) to aMerR exceeding 1,000-fold (Fig. 10F). Taken together, the in vivo and in vitro results examining aMerR interactions with the operator sequence indicate aMerR remains bound to the operator regardless of the presence of the metal ligand. Because aMerR was able to bind the mutant operator in vitro yet unable to mediate repression in vivo, aMerR binding and aMerR-mediated repression are not obligatorily coupled.

DISCUSSION

Mercuric ion, Hg(II), has been shown to inactivate generalized transcription in the archaeon *S. solfataricus* in a specific manner (10). In the data presented here, elevated levels of mercury reductase (MerA) in a *merR* disruption mutant increased transcript abundance of genes unrelated to metal resistance during metal challenge. Since the abundance of these transcripts was shown previously to be reduced by metal exposure in an otherwise-wild-type strain (10), this new finding provides additional evidence that transcription is a primary target of heavy metal toxicity. For this reason, coupling mercury resistance to relief of transcription inhibition represents a unique regulatory response and one that is perhaps specific to members of the archaeal domain that combine bacteria-like mercury resistance genes with a eukaryote-like transcription apparatus.

The wHTH DNA binding domain is a highly conserved sequence motif widely distributed among transcription factors (4). ArsR and MerR constitute two abundant but distinct families of wHTH proteins. A key difference between these two families resides in their response to metal ligands; ArsR proteins dissociate from DNA while MerR proteins remain bound. At the same time, ArsR proteins are generally repressors while MerR proteins both repress and stimulate bacterial transcription initiation frequency. Despite its ability to regulate transcription of mercury resistance genes, aMerR encodes an N-terminal wHTH domain with a short sequence motif related to ArsR family members. The ArsR motif in aMerR, however, lacks the conserved cysteine residue required for ligand-induced DNA release. Despite this divergent feature, the *S. solfataricus* aMerR protein could be the first example of an Hg(II)-responsive ArsR family member.

As an ArsR family member, aMerR should release DNA upon interaction with its cognate metal ligand. While earlier studies found that a strain lacking *merR* exhibited constitutive *mer* expression, indicating aMerR was a transcriptional repressor (24), several types of data presented in this work suggest aMerR instead remains DNA bound during metal challenge, where it confers resistance to transcription inhibition. Northern analysis of *merH* transcript abundance using mercuric reductase-deficient strains examined the role of aMerR on Hg(II) inactivation of *merHp*. Since the absence of aMerR prevented accumulation of *merH* transcript following metal challenge, aMerR is apparently required for initiation of transcription at *merHp*. Secondly, the interaction of aMerR with its DNA binding site in vitro was found to be insensitive to metal addition, something quite unlike ArsR family members (18, 26). Finally, it was shown that an aMerR binding site mutation that relieved repression in vivo did not prevent DNA complex formation in vitro. Since the aMerR binding site is immediately adjacent if not overlapping with the binding sites of generalized transcription factors TFB and TBP, these data suggest aMerR remains promoter bound during metal challenge, where it exerts a protective effect over the preinitiation transcription complex. More elaborate in vivo and in vitro efforts would further clarify the nature of MerR binding.

Interestingly, the *S. solfataricus* aMerR operator spans 31 nt while the bacterial MerR operator spans 18 nt with 7-nt palindromic arms separated by a 4-nt central AT-rich spacer (5). In contrast, the *S. solfataricus* aMerR protein is only 115 residues, while bacterial (*E. coli*) MerR is larger, with 144 residues. This suggests that the *S. solfataricus* aMerR protein either does not require the entire operator for binding or that it binds differently than its bacterial counterpart. The conservation of the *S. solfataricus mer* operator in other *Sulfolobus* species supports an important role for this sequence in mediating transcriptional control of *mer* expression. An internal 16-nt sequence was identified by multiple sequence alignment that could be divided into two halves separated by a variable 2-nt spacer. This suggests the flanking 8-nt half-sites interact with each monomer of a MerR homodimer. The mercury-resistant phenotype produced by the *merR*-IR2 mutation is also consistent with a MerR homodimer. This mutation separated the two halves of the operator by rotating them to different sides of the double helix. Apparently, despite a continued presence of the repeat sequences, MerR was unable to repress *mer* transcription, suggesting monomer interaction may be required for this process. Ongoing studies to examine MerR structure will clarify this issue.

Hg(II)-mediated transient derepression of *mer* expression in *merA* and *merRA* double mutant strains implicates the existence of a secondary system or alternative cellular reductases for metal detoxification. Delayed *mer* induction likely results from the need to reduce initial Hg(II) concentrations below those that block transcription but remain sufficient to relieve

aMerR repression. Following a period of induced expression, *mer* expression is again terminated and is likely to result from further decreases in Hg(II) concentrations below those required for gene induction. Since these strains lack mercuric reductase, the pattern of transient derepression indicates some alternative mechanism operates in these cells that controls Hg(II) levels.

These studies also describe the development and application of several new genetic techniques that expand the crenarchaeal repertoire. Construction of the *merRA* double mutant required the development and use of linear DNA recombination. This modification of earlier methods (15, 24, 31) prevented recombination between two desirable mutations, the *merR* disruption and the *merA* deletion. Earlier methods for targeted recombination employed two successive single-crossover events, which allowed unwanted recombination between desired regions and resulted in loss of the *merA* deleted region. The new approach overcame this constraint by enabling greater control over the crossover event. The second new genetic method developed and used in these studies was a version of allele replacement (7) that is also called markerless exchange. This method was used to construct site-specific mutations in the putative *mer* binding site. Markerless exchange has been used previously for other archaea, accompanied by counterselection (19). As employed in this study, silent mutations were introduced by selection followed by loss of the selectable marker, vector, and unaltered target allele due to spontaneous segregation. The new methods presented here, together with other advances in genetic modification of *S. solfataricus* (28), will promote efforts targeting studies on *Crenarchaeota*.

ACKNOWLEDGMENTS

This research was supported by NSF grants MCB-0085216 and MCB-0235167.

The input of Thijs Ettema and John van der Oost is gratefully appreciated.

REFERENCES

1. **Allen, M. B.** 1959. Studies with Cyanidium caldarium, an anomalously pigmented chlorophyte. Arch. Mikrobiol. **32:**270–277.
2. **Ansari, A. Z., J. E. Bradner, and T. V. O'Halloran.** 1995. DNA-bend modulation in a repressor-to-activator switching mechanism. Nature **374:**371–375.
3. **Ansari, A. Z., M. L. Chael, and T. V. O'Halloran.** 1992. Allosteric underwinding of DNA is a critical step in positive control of transcription by Hg-MerR. Nature **355:**87–89.
4. **Aravind, L., V. Anantharaman, S. Balaji, M. M. Babu, and L. M. Iyer.** 2005. The many faces of the helix-turn-helix domain: transcription regulation and beyond. FEMS Microbiol. Rev. **29:**231–262.
5. **Barkay, T., S. M. Miller, and A. O. Summers.** 2003. Bacterial mercury resistance from atoms to ecosystems. FEMS Microbiol. Rev. **27:**355–384.
6. **Bini, E., V. Dikshit, K. Dirksen, M. Drozda, and P. Blum.** 2002. Stability of mRNA in the hyperthermophilic archaeon Sulfolobus solfataricus. RNA **8:**1129–1136.
7. **Blum, P., D. Holzschu, H. S. Kwan, D. Riggs, and S. Artz.** 1989. Gene replacement and retrieval with recombinant M13mp bacteriophages. J. Bacteriol. **171:**538–546.
8. **Brock, T. D., K. M. Brock, R. T. Belly, and R. L. Weiss.** 1972. Sulfolobus: a new genus of sulfur-oxidizing bacteria living at low pH and high temperature. Arch. Mikrobiol. **84:**54–68.
9. **Condee, C. W., and A. O. Summers.** 1992. A *mer-lux* transcriptional fusion for real-time examination of in vivo gene expression kinetics and promoter response to altered superhelicity. J. Bacteriol. **174:**8094–8101.
10. **Dixit, V., E. Bini, M. Drozda, and P. Blum.** 2004. Mercury inactivates transcription and the generalized transcription factor TFB in the archaeon *Sulfolobus solfataricus*. Antimicrob. Agents Chemother. **48:**1993–1999.
11. **Ettema, T. J., M. A. Huynen, W. M. de Vos, and J. van der Oost.** 2003. TRASH: a novel metal-binding domain predicted to be involved in heavy-metal sensing, trafficking and resistance. Trends Biochem. Sci. **28:**170–173.
12. **Haseltine, C., R. Montalvo-Rodriguez, E. Bini, A. Carl, and P. Blum.** 1999. Coordinate transcriptional control in the hyperthermophilic archaeon *Sulfolobus solfataricus*. J. Bacteriol. **181:**3920–3927.
13. **Haseltine, C., R. Montalvo-Rodriguez, A. Carl, E. Bini, and P. Blum.** 1999. Extragenic pleiotropic mutations that repress glycosyl hydrolase expression in the hyperthermophilic archaeon Sulfolobus solfataricus. Genetics **152:**1353–1361.
14. **Higuchi, R., B. Krummel, and R. K. Saiki.** 1988. A general method of in vitro preparation and specific mutagenesis of DNA fragments: study of protein and DNA interactions. Nucleic Acids Res. **16:**7351–7367.
15. **Hoang, V., E. Bini, V. Dixit, M. Drozda, and P. Blum.** 2004. The role of cis-acting sequences governing catabolite repression control of lacS expression in the archaeon Sulfolobus solfataricus. Genetics **167:**1563–1572.
16. **J. L. Mier, A. B., F. Gonzalez, M. L. Blazquez, and E. Gomez.** 1996. The influence of metallic ions on the activity of Sulfolobus BC. J. Chem. Technol. Biotechnol. **65:**272–280.
17. **Littlefield, O., Y. Korkhin, and P. B. Sigler.** 1999. The structural basis for the oriented assembly of a TBP/TFB/promoter complex. Proc. Natl. Acad. Sci. USA **96:**13668–13673.
18. **Liu, T., S. Nakashima, K. Hirose, M. Shibasaka, M. Katsuhara, B. Ezaki, D. P. Giedroc, and K. Kasamo.** 2004. A novel cyanobacterial SmtB/ArsR family repressor regulates the expression of a CPx-ATPase and a metallothionein in response to both Cu(I)/Ag(I) and Zn(II)/Cd(II). J. Biol. Chem. **279:**17810–17818.
19. **Pritchett, M. A., J. K. Zhang, and W. W. Metcalf.** 2004. Development of a markerless genetic exchange method for *Methanosarcina acetivorans* C2A and its use in construction of new genetic tools for methanogenic archaea. Appl. Environ. Microbiol. **70:**1425–1433.
20. **Reeve, J. N.** 2003. Archaeal chromatin and transcription. Mol. Microbiol. **48:**587–598.
21. **Rockabrand, D., K. Livers, T. Austin, R. Kaiser, D. Jensen, R. Burgess, and P. Blum.** 1998. Roles of DnaK and RpoS in starvation-induced thermotolerance of *Escherichia coli*. J. Bacteriol. **180:**846–854.
22. **Rolfsmeier, M., and P. Blum.** 1995. Purification and characterization of a maltase from the extremely thermophilic crenarchaeote *Sulfolobus solfataricus*. J. Bacteriol. **177:**482–485.
23. **Rolfsmeier, M., C. Haseltine, E. Bini, A. Clark, and P. Blum.** 1998. Molecular characterization of the alpha-glucosidase gene (*malA*) from the hyperthermophilic archaeon *Sulfolobus solfataricus*. J. Bacteriol. **180:**1287–1295.
24. **Schelert, J., V. Dixit, V. Hoang, J. Simbahan, M. Drozda, and P. Blum.** 2004. Occurrence and characterization of mercury resistance in the hyperthermophilic archaeon *Sulfolobus solfataricus* by use of gene disruption. J. Bacteriol. **186:**427–437.
25. **She, Q., R. K. Singh, F. Confalonieri, Y. Zivanovic, G. Allard, M. J. Awayez, C. C. Chan-Weiher, I. G. Clausen, B. A. Curtis, A. De Moors, G. Erauso, C. Fletcher, P. M. Gordon, I. Heikamp-de Jong, A. C. Jeffries, C. J. Kozera, N. Medina, X. Peng, H. P. Thi-Ngoc, P. Redder, M. E. Schenk, C. Theriault, N. Tolstrup, R. L. Charlebois, W. F. Doolittle, M. Duguet, T. Gaasterland, R. A. Garrett, M. A. Ragan, C. W. Sensen, and J. Van der Oost.** 2001. The complete genome of the crenarchaeon Sulfolobus solfataricus P2. Proc. Natl. Acad. Sci. USA **98:**7835–7840.
26. **Shi, W., J. Dong, R. A. Scott, M. Y. Ksenzenko, and B. P. Rosen.** 1996. The role of arsenic-thiol interactions in metalloregulation of the ars operon. J. Biol. Chem. **271:**9291–9297.
27. **Simbahan, J., E. Kurth, J. Schelert, A. Dillman, E. Moriyama, S. Jovanovich, and P. Blum.** 2005. Community analysis of a mercury hot spring supports occurrence of domain-specific forms of mercuric reductase. Appl. Environ. Microbiol. **71:**8836–8845.
28. **Sowers, K. R., P. H. Blum, and S. DasSarma.** Gene transfer in archaea. *In* C. A. Reddy, T. J. Beveridge, J. A. Breznak, G. A. Marzluf, and T. M. Schmidt (ed.), Methods for general and molecular microbiology. American Society for Microbiology, Washington, D.C., in press.
29. **Triezenberg, S. J.** 1992. Preparation and analysis of RNA, p. 4.8.1–4.8.5. *In* F. M. Ausubel, R. Brent, R. E. Kingston, D. D. More, J. G. Seidman, J. A. Smith, and K. Struhl (ed.), Current protocols in molecular biology. John Wiley, New York, N.Y.
30. **Worthington, P., P. Blum, F. Perez-Pomares, and T. Elthon.** 2003. Large-scale cultivation of acidophilic hyperthermophiles for recovery of secreted proteins. Appl. Environ. Microbiol. **69:**252–257.
31. **Worthington, P., V. Hoang, F. Perez-Pomares, and P. Blum.** 2003. Targeted disruption of the α-amylase gene in the hyperthermophilic archaeon *Sulfolobus solfataricus*. J. Bacteriol. **185:**482–488.

Primers	
LacS-KpnI-F	5’ AGTCCGGGGTACCAATACTAGGAGGAGTAGCATATAATTACGT 3’
LacS-KpnI-R	5’ AGTCCGGGGTACCAGTATTAAATCTAAATGACTTTCCAATTAG 3’
merR-L-BamHI-F	5’ ATGCCGCGGATCCATCTTGTGAAAATTAAGGATGCGAT 3’
merR-L-BamHI-R	5’ ATGCCGCGGATCCTCTTGAAAGGCTTGGAAAAATTCTG 3’
merR-R-KpnI	5’ CAAGTTAAATTATCTCATTAGGGTACCATATGTGCTTAGG 3’
merR-R	5’ CACATATGTTCTCGAGATGAGATAATTTAACTTGACC 3’
merI-L-BamHI-F	5’ AGTCCGCGGATCCTTTAGATGCAGCAGGAATCGAATTAAACGA 3’
merI-L-BamHI-R	5’ AGTCCGCGGATCCAGATTATAGATGCCCAATTGAACAAGCTGA 3’
merI-L-BclI-F	5’ AGTCCGCTGATCACTCGATTTCATTTCTTTTTATATAAT 3’
merI-L-KpnI-R	5’ AGTCCGCGGTACCAGATTATAGATGCCCAATTGAACAAG 3’
merI-OL2-XhoI-F	5' GATTATATGAAGATGAGGAACTCGAGGAGATAGCACTCCGTATAAC 3'
merI-OL2-XhoI-R	5' GTTATACGGAGTGCTATCTCCTCGAGTTCCTCATCTTCATATAATC 3'
merI-R	5’ GCTATCTCCTCGACTTCCTCA 3’
merH-L-BamHI-R	5’ AGTCCGCGGATCCCCCTTATCAGTAACTATTATCTTTCCCCCG 3’
merR-BS-OLE-F	5' ATAAGTCTTTCTA(T)GAACATACTAGTGTTCATATGAAAGATTTTTA 3'
merR-BS-OLE-R	5' TAAAAATCTTTCATATGAACACTAGTATGTTC(A)TAGAAAGACTTAT 3'
merR-BS-XbaI-OL-F	5’ AATAAGTCTTTCTATGAACATCTAGATGTTCATATGAAAGATTTTT 3’
merR-BS-XbaI-OL-R	5’ AAAAATCTTTCATATGAACATCTAGATGTTCATAGAAAGACTTATT 3’
merIR-OL-F2	5’ TGATTCTTATCAACTAATATAAAATTTTCACCTATTGACATTATAA 3’
merIR-OL-R	5’ TTTATATTAGTTGATAAGAATCATAAATAGGTGAACTAGATGGTTA 3’
merA-F	5’ GAATTGTACAATTACTCTTCAAAAGT 3’
merA-2F	5’ ATAGGAATTCCAATTCATTTGTAAGAGGCT 3’
merA-R	5’ AGCTACCGGAAGAAAGCCCAATGTAG 3’
merH-2F	5’ TAGGTGGAATTCATGGTTAATCTAAGG 3’
merH-2R	5’ TATCCCAAGCTTGCAACACGATGATACTCC 3’
merH-R	5’ CTATCCCTCTCTAGCAACACG 3’

merI-2F	5’ ATGCAAGAATTCAAGAGATTATATGAAGATGAGG 3’
merI-3R	5’ TTAACTTGATCCAGTACTGCAGCCGCAATAAGCC 3’
merH-PE	5’ ATATATTTCATCTTCGGATAG 3’
merHp-F	5’ ATAGAATTCCAATTCATTTGTAAGAGGCTCC 3’
merHp-R	5’ CGTGTTGCTAGAGAGGGATAG 3’
merR-F	5’ ACCTATTGACATTATAAAACCATGGAGCCTCTTAC 3’